Extraction of underlying multiplicative processes from multifractals via the thermodynamic formalism

Ashvin B. Chhabra, Roderick V. Jensen, and K. R. Sreenivasan
Mason Laboratory, P.O. Box 2159, Yale University, New Haven, Connecticut 06520
(Received 29 December 1988)

This paper describes various procedures for extracting an underlying multiplicative process from the thermodynamic description of multifractals (i.e., its D_q curve), and points out the associated pitfalls of such procedures. We extend previous work by Feigenbaum, Jensen, and Procaccia [Phys. Rev. Lett. **57**, 1567 (1986)] using transfer matrices to the case of singular measures, and develop the corresponding thermodynamic formalism. We find that the extraction procedure based solely on information from the D_q curves allows for an infinity of cascade processes and that additional dynamical information is required to remove this degeneracy. In addition, we find that different multiplicative processes with only three free parameters produce excellent fits to all the D_q curves studied in this paper, which further confuses the inversion process when it is applied to experimental data. We then examine the application of these procedures to a variety of computer and laboratory experiments, such as the period-doubling attractor, the golden-mean circle-map attractor, and a reanalysis of Rayleigh-Bénard experiments corresponding to these examples. Finally we consider laboratory experiments on open flows in two different circumstances. The first deals with velocity measurements in the wake of an oscillating cylinder and has dynamics closely related to that of the circle map. The second case corresponds to the spatial distribution of turbulent energy dissipation in several flows (grid turbulence, wakes, and boundary layers in the laboratory and atmosphere), where the underlying dynamics are presently not well understood. In each of these examples we highlight the above-mentioned ambiguities and, in cases where additional information is available, apply the procedure to extract basic underlying length scales of the phenomena.

I. INTRODUCTION

Fractals seem to be ubiquitous in Nature. There are many objects in physics and mathematics that are characterized by complicated singular functions exhibiting self-similar scaling properties. Two examples of these are the invariant probability distribution on a strange attractor and the natural measure on a Julia set. Mandelbrot[1] introduced the term fractal to describe these complicated sets and singular measures and applied it to a variety of natural phenomena.

The simplest example is the middle-thirds Cantor set defined as the set of points remaining in the unit interval after the middle third is removed, this operation being performed successively on the remaining segments *ad infinitum*. The natural measure associated with this object corresponds to the probability distribution which gives equal weight to each interval at each stage of the construction. Both the set and the measure are described by a single dimension, i.e., the Hausdorff dimension $d_H = \log(2)/\log(3)$.

However, the singular measures associated with most fractals, e.g., the period-doubling attractor, the golden-mean cantorus, the invariant measure on strange attractors and various facets of fully turbulent flows such as the dissipation and enstrophy distributions in real space are described by an hierarchy of different dimensions. These more complex objects are called multifractals.[2,3] The best or most useful way of characterizing them has been the subject of intense study in recent years. As a result, we now have several interrelated formalisms and methods for dealing with them.

In the last few years, it has become a standard procedure to analyze singular measures via this multifractal formalism involving the Renyi dimensions[4,5] D_q and the closely related "singularity spectrum"[3] $f(\alpha)$. The quantities describe scaling properties of *a particular set of measures* (to be described later) that are constructed from the original measure whose properties we seek to describe. They are, in effect, statistical averages that describe macroscopic information about the object and the measures associated with it.

The existence of a multifractal measure often (but not always) indicates an underlying multiplicative process giving rise to it. To make progress towards understanding the physics of complicated, nonlinear phenomena characterized by multifractal measures, one would like to find information on the possible underlying multiplicative processes that could give rise to them. Feigenbaum *et al.*[6] made an important step in this direction, when they showed that a formal mapping between multifractal analysis of fractal sets and conventional thermodynamics (hereafter referred to as the *thermodynamic formalism*) provided a natural way of extracting from the Renyi dimensions some (but not all) of the basic length scales of an underlying multiplicative process.

This paper has three main objectives. First, in Sec. III we extend the approach of Feigenbaum *et al.* for fractal sets to singular measures, and develop the corresponding thermodynamic formalism. Second, in Sec. IV we point

out an important ambiguity in the extracted processes arising from this procedure. In particular one cannot find out the mean number of splittings a of each interval at various levels of refinement solely from the D_q curves. Although a is often assumed to be 2 or the golden mean, choosing different values of a simply gives equivalent three-parameter fits to the D_q curves which also turn out to be excellent approximations to the exact curve. Given any experimental error or just errors arising from box-counting procedures one cannot distinguish these curves from those arising from three-parameter fits that use the correct value of a. Thus to extract the correct underlying multiplicative process one requires additional dynamical information, such as the closest return times, to obtain the correct value of a. Taking these ambiguities into account, we apply in Secs. V and VI the generalized procedure both to computer experiments (generalized Cantor measures) and to four different kinds of laboratory experiments. The first two are Rayleigh-Bénard experiments conducted by Libchaber and co-workers,[7-9] describing the onset of chaos via the quasiperiodic and period doubling routes. The other two are related to the onset of chaos and the description of fully developed turbulence in open flows.[10,11] The onset of chaos is analyzed from single-point velocity measurements in the wake of an oscillating cylinder, where the flow dynamics is closely related to that of the circle map. The second case corresponds to the spatial distribution of turbulent energy dissipation in several flows (grid turbulence, wakes and boundary layers in the laboratory and atmosphere). In all these cases (except for the last) we recover basic information about the dynamics of the underlying multiplicative processes by using additional dynamical information (in the last case only statistical information can be recovered). However, before we do this, we review in Sec. II the formalisms for computing various dimensions, stressing the contexts in which they arise as well as the differences among them.

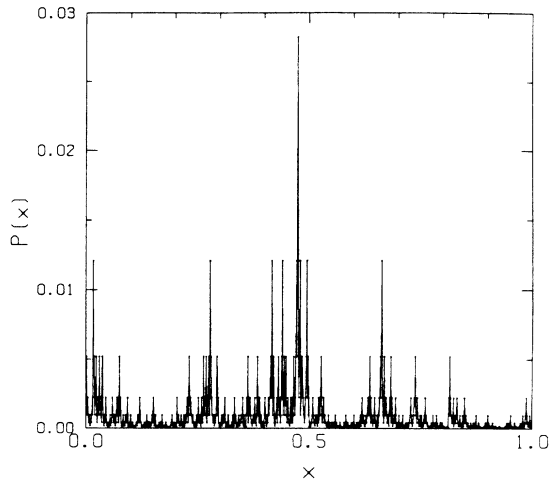

FIG. 1. Measure generated from a two-scale (binomial) measure where at each level of refinement an interval of length L splits up into two intervals of length $L/2$ each, with their probabilities in the ratio of $\frac{7}{3}$. The reason for choosing this specific illustration becomes clear later in Sec. VI B.

II. DIMENSIONS AND THE PARTITION FUNCTION

The starting point for our analysis is a singular measure. Such measures can be created, for example, by iterating a given map such as the logistic or Henon map, and constructing a probability distribution of the relative frequency of visitation in different regions. Another way of creating a singular measure is to consider a multiplicative process where at each stage of construction a unit interval breaks up into intervals of unequal length, each of which contains a given probability. The measure arising from a binary process is shown in Fig. 1. Such a measure is qualitatively similar to those found in experiments as a comparison with Fig. 2 would indicate. If the measure is a complicated singular distribution, then one seeks to exploit possible self similar scaling properties in order to describe it.

To do this one partitions the measure subject to certain constraints. For example, one may choose to partition (cover) the measure with boxes of equal size. The total probability (integrated measure) in each of these boxes would form a set of numbers, an appropriate function of which one seeks to minimize. On the other hand one could choose to partition the measure using boxes of varying size, where the size variation is decided so as to minimize some function of the measure in each of these boxes. Depending on the partitioning (or covering) chosen and on the function that is being minimized one gets different exponents that reflect the scaling properties of the measure, e.g., the box dimension, the Renyi dimensions, the Hausdorff dimension, etc.

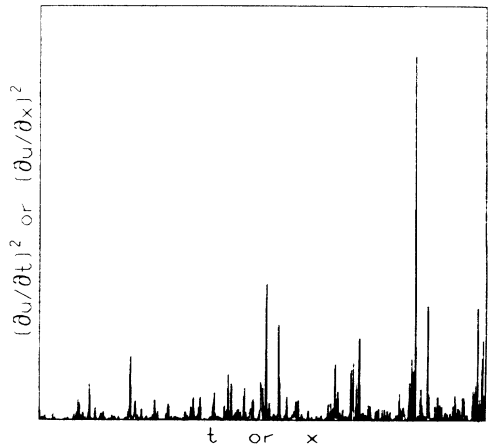

FIG. 2. A sample of data from hot-wire measurements of one-dimensional cuts of the turbulent energy dissipation field in open flows. This particular set of data corresponds to the atmospheric boundary layer at a height of about 2 m above a four-story building. The microscale Reynolds number is of the order of 1600.

A. Hausdorff dimension

If one were interested in computing the Hausdorff dimension of the set of points $\mathcal{M}$ where the dynamical system had visited, one would[12] cover $\mathcal{M}$ with spheres $\{L_i\}$ each of whose diameter (L_i) would be less than or equal to some arbitrary number ρ. This is known as a ρ covering of $\mathcal{M}$. First one defines the function

$$\mathcal{L}_\alpha(\mathcal{M},\rho)=\inf\sum_i (L_i)^\alpha \ , \tag{1}$$

where the infimum is over all the ρ coverings of $\mathcal{M}$. Then the α-dimensional outer measure of $\mathcal{M}$ is defined for positive α by

$$\mathcal{L}_\alpha(\mathcal{M})=\lim_{\rho\to 0}\mathcal{L}_\alpha(\mathcal{M},\rho) \ . \tag{2}$$

The Hausdorff dimension (d_H) of $\mathcal{M}$ is defined by the value of α where $\mathcal{L}_\alpha(\mathcal{M})$ exhibits a discontinuity as a function of α as shown in Fig. 3. Then

$$d_H(\mathcal{M})=\sup\{\alpha:\mathcal{L}_\alpha(\mathcal{M})=\infty\}=\inf\{\alpha:\mathcal{L}_\alpha(\mathcal{M})=0\} \ . \tag{3}$$

B. Partition function of Halsey *et al.*

In a similar spirit, one can analyze a measure using the partition function of Halsey *et al.*[3] First one constructs a ρ covering of the set $\mathcal{M}$. If P_i is the probability (integrated measure) in the ith ball of radius L_i, one considers the function

$$\Gamma_H(q,\tau,\mathcal{M},\rho)=\inf\sum_i \frac{P_i^q}{L_i^\tau} \ , \tag{4}$$

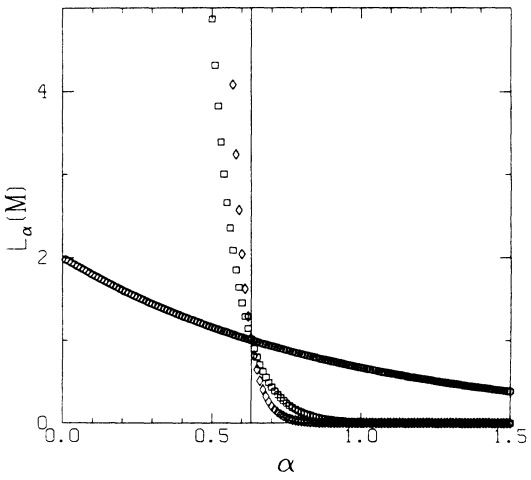

FIG. 3. Determination of the Hausdorff dimension, for the middle-thirds Cantor set. Shown are the L_α outer measures as a function α at three different levels of refinement: □, $n=1$; ○, $n=11$; ◇, $n=21$. Notice that for $\alpha<D_H$ the function monotonically increases with increasing n, while for $\alpha>D_H$ with increasing n the function monotonically decreases to zero. As n increases, the slope of these curves gets steeper and steeper and in the limit of $n\to 0$ the curve approaches the solid line, which is equal to a nonzero constant only for a single value of α, which is the Hausdorff dimension. Note that the L_α outer measure is the same as the partition function at $q=0$.

where q is a real number $(-\infty<q<\infty)$ and the infimum is over all the different coverings. Then one defines

$$\Gamma_H(q,\tau,\mathcal{M})=\lim_{\rho\to 0}\Gamma_H(q,\tau,\mathcal{M},\rho) \ , \tag{5}$$

which is analogous to the α-dimensional outer measure of the set. Following the definition of the Hausdorff dimension, one examines the behavior of $\Gamma_H(q,\tau,\mathcal{M})$ as a function of τ, and defines $\tau^{(H)}$ to be the value of τ where Γ_H jumps from 0 to ∞. Finally, using the definition

$$\tau^{(H)}=(q-1)D_q^{(H)} \ , \tag{6}$$

one can define a set of exponents $(D_q^{(H)})$ that are a set of "generalized dimensions." When $q=0$, $-\tau^{(H)}=D_0^{(H)}=D_H$ is the Hausdorff dimension of the set $\mathcal{M}$. As seen above, the correct value of $\tau^{(H)}$ is defined as that which makes the value of $\Gamma_H(q,\tau,\mathcal{M})$ (also known as the partition function) finite. Any other value of $\tau^{(H)}$ would make the infinite sum defining Γ_H diverge or go to zero. This statement is also illustrated in Fig. 3 where the ordinate corresponds to the partition function for $q=0$ for the middle-thirds Cantor set for different values of $\tau^{(H)}$ at various levels of construction. Clearly this procedure (in the limit of the number of levels going to infinity) picks out a unique value of $\tau^{(H)}$ as demanded by the definition. At this particular value of $\tau^{(H)}$ (which happens to be the negative of the Hausdorff dimension of the set) the partition function is finite and equal to some constant. By convention we assign this finite constant the value unity; any other finite value would not change the dimension. In Fig. 4 we compute the partition function for $q=2$, showing that once again a unique value of $\tau^{(H)}$ is picked out. In this case this value is related to what is known in the literature as the correlation dimension. For the middle-thirds Cantor measure, the Hausdorff dimension and the correlation dimension are equal.

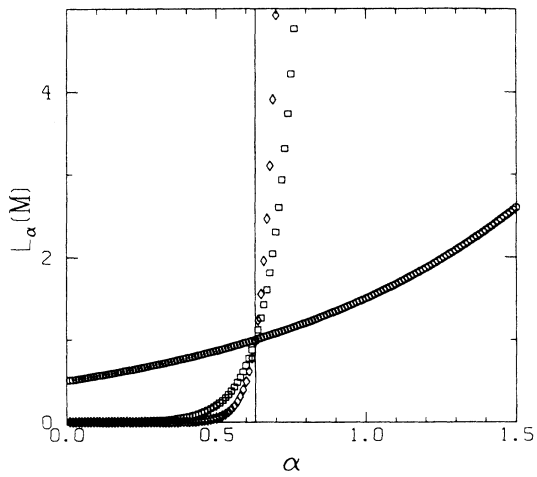

FIG. 4. Same as Fig. 3 except the partition function is calculated using the value $q=2$. The behavior in the limit $n\to 0$ is identical to that in Fig. 3 except the unique value of α for which the partition function is finite and nonzero gives us the correlation dimension (D_2).

C. Generalized box dimensions

The Hausdorff dimension is extremely difficult to compute. Given no knowledge of the multiplicative process leading to the construction of the measure it is often impossible to find the best covering as it involves an infimum over all possible coverings. Thus a simpler or different definition of dimension is needed. The definition usually used is that of the box dimension first defined by Bouligand[13] and later popularized and applied to data from a variety of phenomenon by Mandelbrot.[1] Here one covers the attractor with balls or boxes of *equal* size (say, L), and constructs a measure by counting the number of points in each box. The box size is reduced and the procedure repeated to obtain d_{box} which is defined as

$$d_{\text{box}} = \lim_{L\to 0} \frac{\log N(L)}{\log(L^{-1})} , \tag{7}$$

where $N(L)$ is the number of boxes of size L that have at least one point in it. It is important to note that the box dimension does not involve an infimum over all coverings, and thus is essentially a different dimension from the Hausdorff dimension. Much confusion[14] has arisen by the practice of denoting the box dimension and other dimensions collectively as fractal dimensions. One must explicitly state which dimension one is computing as they may vary considerably from each other. An example of this would be the set of rational numbers on the real line, for which $d_{\text{box}}=1$ but $d_H=0$.

The Renyi-Hentchel-Procaccia dimensions (also known as "generalized dimensions") are defined by considering an approximation to the partition function of Halsey *et al.*, by considering a uniform covering of the set (i.e., $L_i=L$) rather than a minimum covering. The partition function then simplifies to

$$\Gamma(q,\tau,L)=\sum_i \frac{P_i^q}{L^\tau}=\text{const} . \tag{8}$$

We can let the constant equal unity without affecting the value of the dimensions. Then using the relation $\tau=(q-1)D_q$, and taking logarithms of both sides, we can rewrite Eq. (8) as

$$D_q=\frac{1}{q-1}\lim_{L\to 0}\frac{\log\sum_i P_i^q(L)}{\log(L)} . \tag{9}$$

It is important to remember that in this definition the partition function has been simplified to considering partitions (or boxes) of equal size. One is then computing a set of "generalized dimensions" that are different but closely related to the set of $D_q^{(H)}$'s defined by Halsey *et al.* We will call these "generalized box dimensions" hereafter. In the definition of Halsey *et al.* $D_0^{(H)}$ was the Hausdorff dimension. Here D_0 gives us the box dimension. The general inequality

$$D_q \geq D_q^{(H)} \tag{10}$$

holds for all q.

Similarly, when dealing with maps, one often constructs a special partition which deals with boxes of equal probability, but unequal lengths. One can do this by arbitrarily choosing a constant (say, P) that would be the probability contained in each box, and integrating the singular measure until that constant was reached, thus defining a length (box size). Doing this over the entire measure would give us a set of lengths that would then enable us to compute a set of D_q's similar to the Renyi dimensions. (It should be noted that such a nonoverlapping procedure is only defined in one dimension. In higher dimensions the balls covering the set would overlap.) This is equivalent to putting $P_i=P$ in the Halsey partition function. This would then give the implicit equation

$$\sum_i L_i^{-\tau}=P^{-q} , \tag{11}$$

which determines the value of D_q in the limit of $P\to 0$.

In some cases if we have sufficient information on the dynamics of the system we can find the minimum covering of the attractor. This can be done for example for period doubling and the quasiperiodic transition to chaos in the sine circle map. Then the computed values of D_q will correspond to the set of dimensions $D_q^{(H)}$ defined by Halsey *et al.* However, most of the time one does not know how to find such a covering, and one must work with arbitrarily defined equal box sizes (or equal increments of probability). In particular one usually uses equal box sixes as one does not have to solve the implicit equation that arises when P is fixed.

D. An example

We will now illustrate these fundamental concepts of the multifractal formalism by applying them to the measure shown in Fig. 1, which was generated by a multiplicative process defined by dividing the unit interval into two pieces of half the original length and giving them each a probability of 0.7 and 0.3, respectively. This process is carried out repeatedly, giving rise to a multifractal measure. There are several ways of calculating the D_q curve of such a measure. The simplest is to use the partition function in Eq. (8). We know that the length of each piece is $L_i=2^{-n}$. The probabilities in each of the pieces (or boxes) is given by one of the realizations of $(p_1+p_2)^n$, i.e., equal to $P_i=p_1^k p_2^{n-k}$, where $k=0,1,\ldots,n$. The total number of pieces is given by $N_n=2^n$. On substituting these and setting the constant to unity, we get

$$\sum_i^{N_n} P_i^q=(p_1^q+p_2^q)^n=(0.7^q+0.3^q)=2^{-n\tau} . \tag{12}$$

Thus for each value of n we can solve for $\tau(q)=-\log_2(0.7^q+0.3^q)$. Then one can find the D_q curve from $\tau(q)=(q-1)D_q$. This yields the curve shown in Fig. 5.

It is, however, important to remember that when such dimensions are calculated for physical data, the limit $L\to 0$ is never taken. This is because fractal behavior in nature exists only over a finite range of scales below which the underlying physics changes and such scaling no longer holds. One therefore usually looks for a region where such scaling holds and calculates an exponent that is analogous to a dimension in the limit $L\to 0$.

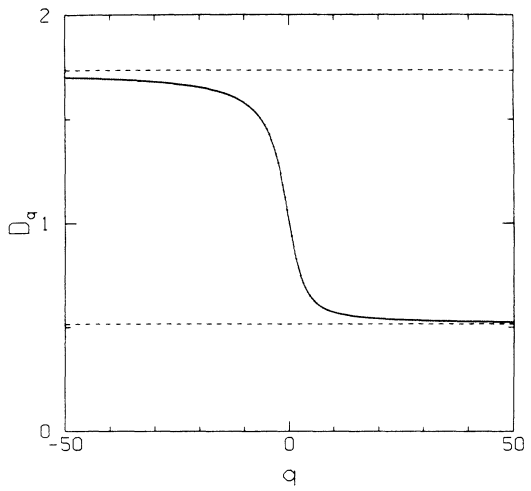

FIG. 5. D_q curve for the binomial measure shown in Fig. 1.

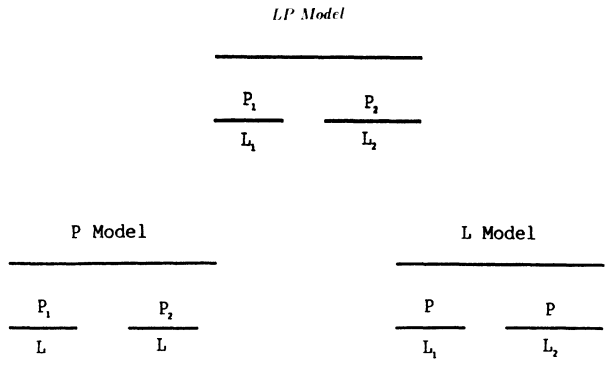

FIG. 6. Schematic diagram of the three binary processes: An LP process, a P process, and an L process.

III. TRANSFER-MATRIX TECHNIQUE

There are several deep connections between dynamical systems on the one hand and statistical mechanics on the other. Some of these have been developed in some detail.[15–17] We will, however, restrict ourselves to a more elementary analogy between the multifractal description[4,3,18,17,19] and the evaluation of thermodynamic quantities in equilibrium statistical mechanics. In this section we will elaborate on this formal analogy, and extend the work of Feigenbaum *et al.*[6] on the extraction of information about an underlying dynamical process via the thermodynamic formalism.

In practice there are a variety of different procedures for associating a multiplicative process with a singular measure. For example, one can choose to cover the measure with boxes (or balls) of equal length (radius), i.e., letting the probabilities in each of the boxes vary. Then a multiplicative process modeling this would, at each level of refinement, be required to have boxes sizes of equal length (which decreases with some constant factor at each level of refinement) with the probabilities in each of these boxes varying in some nontrivial fashion reflecting the complexity of the measure. We call such a multiplicative process a P model. Alternatively one could choose to cover the measure by using boxes of equal probability, i.e., letting the lengths vary in some nontrivial fashion. Such a process can be modeled by a multiplicative process where at each level of refinement the probabilities in each box reduce by a constant factor while the lengths vary in a fashion reflecting the properties of the measure. We will call such a multiplicative process an L model. Finally, one can let both the length and the probability in each box vary according to some criterion. We will call a multiplicative process that models such a refinement process an LP model. (These three multiplicative processes are illustrated schematically in Fig. 6.) Feigenbaum considered L models of singular measures associated with one-dimensional maps. Here we first review the approach of Feigenbaum *et al.* and then extend the method to P models (and to LP models in Appendix B).

A. L models

Consider a multiplicative process where at each level of refinement each interval splits into a pieces which in general are of different lengths. Then at the nth level of refinement this process will generate a measure which can be naturally divided into $N_n = a^n$ different boxes of length L_i $(i = 1,2,\ldots,a^n)$ with equal probability $P_i^{(n)} = N_n^{-1} = a^{-n}$ in each box. The partition function at this level is

$$\Gamma^{(n)}(q,\tau) = \sum_{i=1}^{N^n} \frac{(P_i^{(n)})^q}{(L_i^{(n)})^\tau} = \sum_{i=1}^{a^n} \frac{a^{-nq}}{(L_i^{(n)})^\tau} . \tag{13}$$

Since the partition function can, without loss of generality, be equated to unity, we can write

$$\sum_{i=1}^{a^n} (L_i^{(n)})^{-\tau} \equiv \sum_i e^{-\tau E_i^{(n)}} = (P_i^{(n)})^{-q} = a^{nq} \equiv a^{-nF(\beta)} , \tag{14}$$

where we have defined a new variable

$$E_i^{(n)} = -\ln(L_i^{(n)}) . \tag{15}$$

In thermodynamics the partition function is the sum of Boltzmann probabilities, each of which is expressed as an exponential raised to the product of an inverse temperature β and an energy of a possible configuration of the system. Thus one can identify E_i as the energy of a particular configuration of the system. The partition function can also be expressed as exponential times a "free energy." Therefore in Eq. (14) we can identify[17]

$$F(\beta) = -q \tag{16}$$

with a free energy [times a constant $\ln(a)$] which depends on the inverse temperature

$$\beta = -\tau . \tag{17}$$

Moreover, the generalized box dimensions D_q and q can be expressed in terms of β and $F(\beta)$ as[17]

$$D_q = \frac{\beta}{1+F(\beta)} \ . \tag{18}$$

As this thermodynamic analogy would suggest, the D_q's are statistical averages, reflecting the average scaling properties of the natural measure. Thus there is a loss of certain details of the dynamics. This has been earlier emphasized by Feigenbaum.[17] On the other hand, the microscopic information about a deterministic multiplicative dynamical system and its scaling properties is contained in a scaling function,[20] which describes the scalings or contractions of the various elements of the attractor in time.

When working in the framework of a tree structure where each (parent) interval gives rise to a certain number a of (offspring) intervals at the next level of refinement, the various values of the scaling function are simply the ratio of the offspring to parent intervals of the various branches. For example, the attractor at the period-doubling accumulation point can be thought of as generated by the successive refinements of a measure created from periodic orbits at the superstable period doublings. The intervals at each level are formed by joining nearest-neighbor points, thus constructing a measure by giving equal weight to each such interval. The scaling function which describes the contraction factors of each interval along each branch is defined as

$$\sigma_l(\epsilon_{n+1},\ldots,\epsilon_0)=\frac{L(\epsilon_{n+1},\ldots,\epsilon_0)}{L(\epsilon'_n,\ldots,\epsilon'_1,\epsilon_0)}\delta_{\epsilon_n,\epsilon'_n}\cdots\delta_{\epsilon_1,\epsilon'_1} , \tag{19}$$

$L(\epsilon_n,\ldots,\epsilon_0)$ being the length of an interval belonging to the tree. For the period-doubling case the ϵ_i are binary digits that describe the location of that interval in the tree structure. The problem is that the construction of the scaling function requires *a priori* knowledge about the underlying dynamics for it is a concise codification of the dynamics. For most nonlinear systems of interest (e.g., fully developed turbulence), such information is not readily available.

The attractive feature of the multifractal formalism is that its analysis can be adapted successfully to systems whose dynamics may be known to varying degrees, or perhaps even completely unknown. Given experimental signals one can easily compute the D_q curve and compare it with those from model multiplicative processes. From such comparisons one can deduce certain statistical characteristics of the systems, or of the same system at different parameter values, and infer features of the dynamical processes leading to the observed macroscopic characteristics. The method proposed by Feigenbaum and others is then a way to extract *parts* of the scaling function from the Renyi dimensions of the attractor. For clarity and completeness, we recapitulate their method with some additional comments.

As described earlier, we begin with a measure that has been suitably partitioned by considering boxes of equal probability. This is done at two successive levels of some implicitly assumed hierarchy (e.g., the supercritical period doublings of the period-doubling attractor, or successive Fibonacci approximants of the golden-mean circle-map attractor). One assumes typically that the number of boxes N_n required to cover the fractal will grow exponentially with each level of refinement, and that one can define a number a such that $N_n = a^n$. At the nth level $P_i^{(n)} = N_n^{-1}$, which implies

$$\Gamma^{(n)}(\tau) = \sum_{i=1}^{N_n} (L_i^{(n)})^{-\tau} = a^{nq} \ . \tag{20}$$

If we take the ratio of this partition function at two successive levels [say, the $(n+1)$th and the nth], we have

$$\frac{\Gamma^{(n+1)}(\tau)}{\Gamma^{(n)}(\tau)} = \frac{\sum_{i=1}^{N_{n+1}} (L_i^{(n+1)})^{-\tau}}{\sum_{i=1}^{N_n} (L_i^{(n)})^{-\tau}} = a^q \ . \tag{21}$$

By making use of the Feigenbaum scaling function defined earlier and substituting this in Eq. (21) we get

$$\sum_{(\epsilon_{n+1}\cdots\epsilon_0),(\epsilon'_n,\ldots,\epsilon_0)} \delta_{\epsilon_n,\epsilon'_n}\cdots\delta_{\epsilon_1,\epsilon'_1}\sigma_l^{-\tau}(\epsilon_{n+1},\ldots,\epsilon_1,\epsilon_0)[L(\epsilon'_n,\ldots,\epsilon'_1,\epsilon_0)]^{-\tau} = \lambda(q) \sum_{(\epsilon_n,\ldots,\epsilon_0)} [L(\epsilon_n,\ldots,\epsilon_1,\epsilon_0)]^{-\tau} \ , \tag{22}$$

where the $\delta_{\epsilon_n,\epsilon'_n}$ are the conventional Kronecker delta's. Here $\lambda(q)=a^q$ is the leading eigenvalue of the transfer matrix T, which is defined in terms of the scaling function as

$$T_{(\epsilon_{n+1},\ldots,\epsilon_0),(\epsilon'_n,\ldots,\epsilon_0)} = \sigma_l(\epsilon_{n+1},\ldots,\epsilon_0)^{-\tau} \times \delta_{\epsilon_n,\epsilon'_n}\cdots\delta_{\epsilon_1,\epsilon'_1} \ . \tag{23}$$

Given τ as a function of q, one can then recover certain basic length scales by requiring that a^q be the leading eigenvalue of T (see Appendix A). The reason for considering only the leading eigenvalue is that one can express the partition function as the trace of the product of n such transfer matrices. One then assumes that as $n \to \infty$ the leading eigenvalue will dominate over all the others.

In general, the transfer matrix will be an $\infty \times \infty$ matrix. Each element of this matrix reflects a scaling factor of the dynamical process. To get a first-order approximation to the dynamics of the system, one uses a severely truncated finite matrix (often 2×2 or 4×4) to solve these equations. In the simplest case one approximates the transfer matrix with a 2×2 matrix, whose eigenvalues are determined by the characteristic equation

$$\lambda^2(q,\tau) - \lambda(q,\tau)\,\mathrm{Tr}[T] + \mathrm{Det}[T] = 0 \ . \tag{24}$$

The model we choose can be represented by a transfer matrix whose leading eigenvalue as a function of q can be

computed (see Appendix A). Having done this one can then extract from the $\tau(q)$ curve the leading length scales of the model. The model can be refined and more details of the underlying structure that gave rise to the measure can be discerned. Usually the finite precision of the experimental data places severe constraints on the possibility of further refinements. In Appendix A we give details of the procedure to calculate the D_q curves for all of the L models considered in this paper.

B. *P* models

P models visualize multifractal measures as arising from a process that merely rearranges probability as the cascade proceeds, diminishing on some boxes and increasing on others.

If we do not know much about the underlying physical process, and are faced with multifractal measures whose construction one cannot control, then the P model is natural. Indeed it is the P models of Ref. 18 in turbulence that led to the earliest multifractal descriptions. In addition, the box-counting method of computing dimensions implicitly assume P models, as they consider the scaling of boxes of equal length at each stage of construction or refinement. We will now develop the corresponding thermodynamic analogies for the P model.

Consider the case where the measure is being rearranged on the continuum. (Assuming that it is being rearranged on a fractal set will simply introduce another constant related to the Hausdorff dimension of that set; see Appendix A.) Box counting with N_n boxes of equal size implies $L_i^{(n)}=N_n^{-1}$. Taking the Halsey partition function to be unity allows one to introduce a partition function

$$\Gamma^{(n)}(q)=\sum_{i=1}^{N_n}(P_i^{(n)})^q=(N_n^{-1})^\tau , \tag{25}$$

where $P_i^{(n)}$ is the probability in the ith box at the nth level. In addition one can assume that typically the number of boxes required to cover the fractal will grow exponentially with each level of refinement. Thus one can define a number a such that $N_n=a^n$. Defining an energy by

$$E_i^{(n)}=-\ln(P_i^{(n)}) , \tag{26}$$

we can, at the nth level, write the partition function as

$$\Gamma^{(n)}(q)=\sum_{i=1}^{a^n}[P_i^{(n)}]^q\equiv\sum_{i=1}^{a^n}e^{-(qE_i)} . \tag{27}$$

From Eq. (27) it follows that

$$\Gamma^{(n)}(q)=a^{-n\tau}=e^{-nF(\beta)/\ln(a)} , \tag{28}$$

which then leads to the following thermodynamic identifications:

$$\beta=q , \tag{29}$$

$$F(\beta)=\tau . \tag{30}$$

Furthermore, one can define D_q by

$$D_q=\frac{F(\beta)}{\beta-1} . \tag{31}$$

Thus q is related to the inverse temperature and τ is a free energy times a constant $[\ln(a)]$, and we have according to convention[17] absorbed the β term in the free energy.

We now outline the procedure for extracting scaling information corresponding to P models. If we take the ratio of the partition function at two successive levels of refinement [say, the $(n+1)$th and the nth] then

$$\frac{\Gamma^{(n+1)}(q)}{\Gamma^{(n)}(q)}=\frac{\sum_{i=1}^{N_{n+1}}(P_i^{(n+1)})^q}{\sum_{i=1}^{N_n}(P_i^{(n)})^q}=a^{-\tau} . \tag{32}$$

We then define a scaling function for measures σ_p,

$$\sigma_p(\epsilon_{n+1},\ldots,\epsilon_0)=\frac{P(\epsilon_{n+1},\ldots,\epsilon_0)}{P(\epsilon_n,\ldots,\epsilon_0)}\delta_{\epsilon_n,\epsilon_n'}\cdots\delta_{\epsilon_1,\epsilon_1'} , \tag{33}$$

where $P(\epsilon_n,\ldots,\epsilon_0)=P_i^{(n)}$. The subscript i represents the probability in the ith box and its location on the nth level of the tree is given by the string of n ϵ_i's, each of which takes on a value representing the path chosen in the tree. Our definition of σ_p in the context of multifractal measures is the natural analog of the Feigenbaum scaling function σ_I. Substituting this definition of the scaling function in the previous equation we have

$$\sum_{(\epsilon_{n+1},\ldots,\epsilon_0),(\epsilon_n',\ldots,\epsilon_0)}\delta_{\epsilon_n,\epsilon_n'}\cdots\delta_{\epsilon_1,\epsilon_1'}[\sigma_p(\epsilon_{n+1},\ldots,\epsilon_0)]^q[P(\epsilon_n',\ldots,\epsilon_1',\epsilon_0)]^q=\lambda(-\tau)\sum_{(\epsilon_n,\ldots,\epsilon_0)}[P(\epsilon_n,\ldots,\epsilon_0)]^q , \tag{34}$$

where the Kronecker delta's $\delta_{\epsilon_n,\epsilon_n'}$ once again serve the purpose of comparing only the ratios arising from intervals and their direct successors. Here $\lambda(-\tau)=a^{-\tau}$ is the leading eigenvalue of the transfer matrix defined as

$$T_{(\epsilon_{n+1},\ldots,\epsilon_1,\epsilon_0),(\epsilon_n',\ldots,\epsilon_1',\epsilon_0)}=\sigma_p^q(\epsilon_{n+1},\ldots,\epsilon_1,\epsilon_0)\delta_{\epsilon_n,\epsilon_n'}\cdots\delta_{\epsilon_1,\epsilon_1'} . \tag{35}$$

Then given τ as a function of q, one can recover certain basic contraction ratios (which are the elements of the transfer matrix) by requiring that a^q be the leading eigenvalue of T. In Appendix A we explain how the D_q curves were calculated for P-model examples considered in this paper.

IV. ANALYSIS OF A GENERALIZED CANTOR MEASURE

There are two questions one might ask at this point. First, do these D_q or $\tau(q)$, curves, uniquely determine the

nature of the multiplicative process? Is it possible to construct an identical D_q curve from two different processes one of which may assume equal probabilities in boxes of varying length (i.e., an L model) and the other which may assume equal box sizes with varying probabilities (i.e., a P model). This question is directly related to the fact that given a measure at a certain stage, one usually has no idea on how to correctly partition it. In general one assumes either equal P_i's or equal L_i's. Secondly, do these curves uniquely determine the dynamics of the process, e.g., is it possible to arrive at an identical D_q curve for a binary process (i.e., dynamics similar to the period-doubling route to chaos) from a model with the dynamics of a golden-mean process (i.e., dynamics similar to the quasiperiodic route to chaos discussed in Appendix A)? We will seek answers up to some finite precision, as the primary motivation comes from the desire to extract the underlying multiplicative processes for experimental systems.

We first examine a (two-scale) generalized Cantor measure. At each successive level of refinement, each piece breaks up into two pieces of unequal length and unequal measure. We arbitrarily choose $L_1=0.1475$, $L_2=0.830$, $P_1=0.30$, and $P_2=0.70$. Thus the multiplicative process can be represented by a 2×2 transfer matrix where each contraction ratio is denoted by two digits, the leftmost digit indicating if the interval was to its left or right of its parent, and the second digit does the same for the parent interval (see Appendix B),

$$\sigma_l(00)=\sigma_l(01)=L_1 , \tag{36}$$

$$\sigma_l(10)=\sigma_l(11)=L_2 , \tag{37}$$

$$\sigma_p(00)=\sigma_p(01)=P_1 , \tag{38}$$

$$\sigma_p(10)=\sigma_p(11)=P_2 . \tag{39}$$

We call this an LP model (as both the length and probabilities contraction factors depend on the position of each piece) with no memory (as the contraction factors are decided solely on whether the offspring is to the right or left of its parent, and is independent of its parent's position). The D_q and $\tau(q)$ curves for this process can be calculated analytically and numerically. We thus (by construction) explicitly know the true underlying multiplicative process that generates a measure whose scaling properties are given by the analytically calculated D_q or $\tau(q)$ curves. We can now answer the two questions raised before.

First consider alternative models for the underlying multiplicative processes. The simplest nontrivial model is a two scale L or P multiplicative process with no memory. If we consider an L model with no memory, i.e.,

$$\sigma_l(00)=\sigma_l(01)=L_1 , \tag{40}$$

$$\sigma_l(10)=\sigma_l(11)=L_2 , \tag{41}$$

$$P_1=P_2=\tfrac{1}{2} , \tag{42}$$

we are unable to get good fits to the above D_q curve from such a model (as highlighted by the middle portion of Fig. 7 for one particular case) no matter what parameters of L_1 and L_2 we choose. We find the same result for the D_q curve obtained from a two-scale P model with no memory, i.e., with

$$\sigma_p(00)=\sigma_p(01)=P_1 , \tag{43}$$

$$\sigma_p(10)=\sigma_p(11)=P_2 , \tag{44}$$

$$L_1=L_2=\text{const} . \tag{45}$$

Therefore we must refine our model, incorporating a one time-step memory in the process.

Consider an L model, with $\sigma_l(00)\neq\sigma_l(01)$ and $\sigma_l(10)\neq\sigma_l(11)$. This introduces one more free parameter in our fit [as only the product $\sigma_l(01)\sigma_l(10)$ appear in the calculation of the d_q curves]. Computing the D_q curve from such a model and plotting it against the D_q curve of the given generalized Cantor measure, we find in Fig. 8 excellent agreement over all regions. The same is true for a refined P model, i.e., with $\sigma_p(00)\neq\sigma_p(01)$ and $\sigma_p(10)\neq\sigma_p(11)$ (Fig. 8). This is remarkable because in the models with one time-step memory we used the values of D_∞, D_0, and $D_{-\infty}$ to determine L_1, L_2, and P for an L model, and P_1, P_2, and L for a P model. That is, although we matched the two curves only at three points the agreement is excellent over all regions. To within experimental accuracy one would not be able to distinguish between the three curves. We conclude that the D_q formalism (as used presently) cannot distinguish between LP processes from just L or P processes with one time-step memory.

To answer our second question, we first note that the example being considered is clearly a binary process (i.e.,

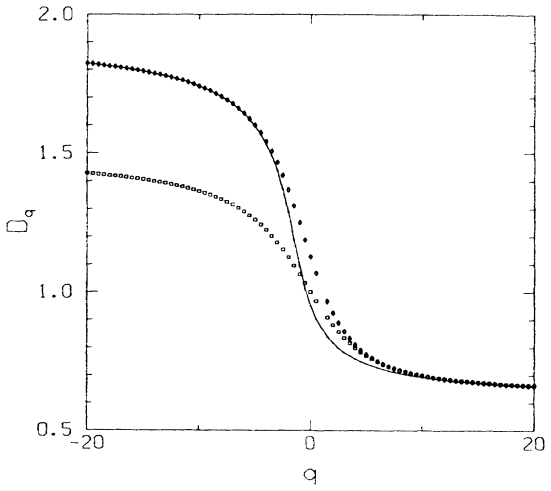

FIG. 7. The D_q curve for an LP model (solid line) and its comparison with a two-scale L model (diamonds) and a two-scale P model (squares). This corresponds to a 2×2 transfer matrix with no memory so that $\sigma(01)=\sigma(11)$ and $\sigma(10)=\sigma(00)$, thus reducing the number of free parameters to two.

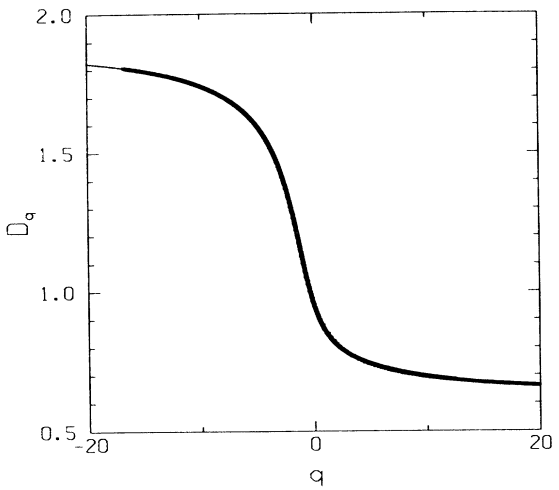

FIG. 8. The D_q curve for an LP model (squares) and its comparison with an L model (circles) and a P model (diamonds), both with $a=2$, 2×2 transfer matrix (TM) for the generalized Cantor measure. The differences (if any) are not discernible on the graph.

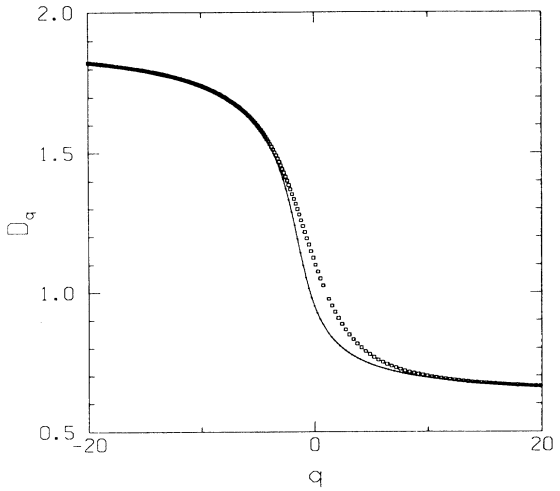

FIG. 9. The D_q curve for an LP model (solid line) and its comparison with an L model (squares) with $a=g$, 2×2 TM. The latter model has only two free parameters and thus one cannot fit the entire curve.

$a=2$) by construction. The question then arises if models with $a=(\sqrt{5}+1)/2$ (i.e., the golden-mean denoted by g) are able to replicate the given D_q curve. We first try the simplest model, i.e., an L model with one time-step memory, that has one of its diagonal elements equal to zero in its transfer-matrix representation. This requires that $a=g$ (see Appendix A). In Fig. 9 we show a comparison between the D_q curve for the generalized Cantor measure with $a=2$ with the D_q curve for an L model with $a=g$. Note that although the two end regions fit quite well, the central region does not. The reason for this is that an L model represented by a 2×2 transfer matrix with one of its elements equal to zero has only two free parameters. Thus we could only match two points from the curve, which we chose to be D_∞ and $D_{-\infty}$. However, going to higher-order approximations gives us more parameters. A 4×4 transfer matrix (a model with two time steps memory) with $a=g$ has three free parameters, enabling us to match D_0 as well. The excellent agreement (shown in Fig. 10) between the two D_q curves arising from models with $a=2$ and $a=g$, respectively, tells us that this formalism cannot find a unique value of a. Therefore to correctly reproduce the dynamics of the underlying multiplicative process, one must determine the value of a from some other information.

The above examples tell us that the crucial ingredient for a good fit is the number of free parameters in the model, not the value of a, nor the nature of the multiplicative model (i.e., P, L, or LP). Furthermore, having chosen a value of a, it is remarkable that we need only three free parameters to fit the entire D_q or $\tau(q)$ curves in each of the examples considered so far in this paper.

Lest the reader be misled that all D_q curves can be exactly fitted by three free parameters we provide a simple counterexample that will show that while we do not get exact fits we get excellent approximations to the exact curves. The accuracy of these approximations are almost always better than the curves obtained by box-counting experimental or computer-generated data where the errors of finding straight lines from log-log plots can be quite large. Our counterexample to illustrate this point is a five-scale Cantor measure where at each stage of refinement each interval breaks up into five smaller pieces of equal length but unequal probability. A curve generated by a binary L model with three free parameters is shown in Fig. 11. The fits are quite good, except in the region near $q=0$ where small differences exist. Blowing up the D_q curve of Fig. 11 in a small region around $q=0$

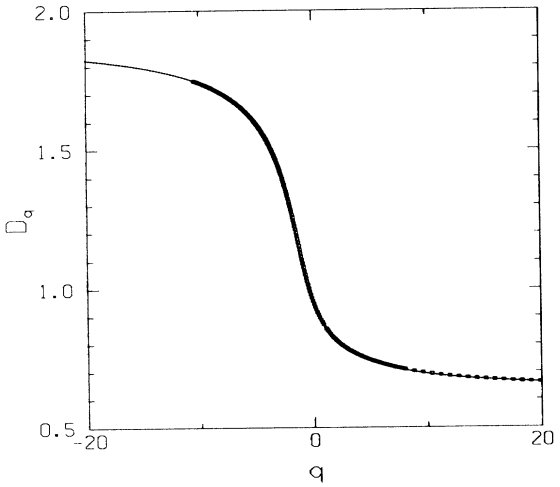

FIG. 10. The D_q curve for an LP model (solid line) and its comparison with an L model (squares) with $a=g$, 4×4 TM. As a consequence of going to the next order of the transfer matrix the latter model has three free parameters, and one can fit the entire curve to great accuracy.

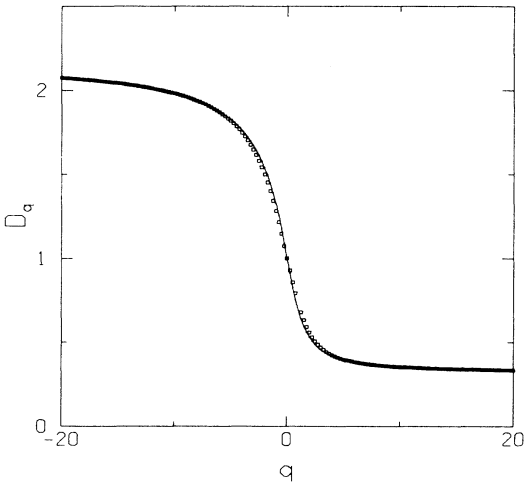

FIG. 11. The D_q curve for a five-scale P model (solid line) ($P_1=0.03$, $P_2=0.05$, $P_3=0.08$, $P_4=0.60$, and $P_5=0.24$) and a three parameter approximation to it (squares).

shows us in Fig. 12 that the exact and the approximate curve differ by a small amount in a small region around $q=0$. This difference, however, is small for most curves and well within the usual experimental error.

We are thus faced with a perplexing number of models, all of which have D_q curves that are indistinguishable (within some accuracy) at the level of the thermodynamic data that we are trying to fit. It is important to emphasize that as we go to further and further refinements of these models, all the fits simply get better. This is because we are just increasing the number of free parameters that can be adjusted to fit the given data.

We now discuss why the value of a is ambiguous. In

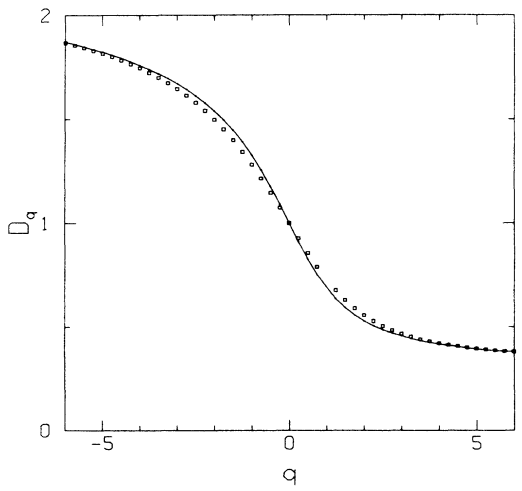

FIG. 12. Enlargement of the region around $q=0$ for Fig. 11. Notice the systematic differences between the exact curve (solid line) and the three-scale approximation (squares). These differences, however, are much less than the error bars characteristic of box-counting procedures applied to experimental or computational data.

the transfer-matrix formalism, we compared the partition functions at two successive levels of refinement [Eq. (21)]. The right-hand side of the equation was

$$\frac{N_{n+1}^{-1}}{N_n^{-1}}=\frac{a^{-(n+1)}}{a^{-n}} . \tag{46}$$

This then gave us a value for a. The problem is that given a measure for some arbitrary system, whose dynamics is not known, one has no idea how to correctly define two successive levels of refinement. The only piece of information one has is the number of points in the measure at some unknown level of refinement. Thus we only know the value of N_{n+1} and are really free to choose N_n. By suitable choices of N_n one can get almost any value of a.

This is a rather crucial point in our argument, so we elaborate on it. Consider the tree picture. We have two unknowns: a, which is the mean number of further branchings at each level, and n, which is the level of refinement. Thus the ratio N_{n+1}^{-1}/N_n^{-1} can be rewritten as $a^{-(n+1)}/a^{-(n)}$, which would provide us with the true dynamics, or as $b^{-(m+1)}/b^{-(m)}$, which would be equally valid, given our thermodynamic information. Such a choice would define a multiplicative process that would result in the same measure, but the wrong dynamics.

The result of the above argument is that one cannot blindly extract the leading scales of the underlying multiplicative process from the thermodynamic information. One needs to establish a unique value of the parameter a. This always comes from elsewhere. By knowing something about the underlying dynamics one can make a judicious choice of a, after which this formalism can be applied. Failing this, the formalism merely presents an (infinite) catalog of models, each of which leads to the construction of the measure under study, but need not replicate the correct dynamics.

The other ambiguity we have exposed is the choice of a P or L model. In turbulence, for example, the P model has been used by Mandelbrot[18] and by Meneveau and Sreenivasan[10] for the dissipation distribution in fully developed turbulence. The L model is used to describe the onset of chaos in Rayleigh-Bénard cells[9,7] and in open flows.[11] There seems to be no way of finding out purely from the statistical (thermodynamic) information how the measure was built up and what model is more correct or useful in describing this process.

As already remarked, additional information is required to make such a choice. For example, if one knows the dynamics of the process, i.e., if one can figure out how to define successive levels of refinement, then it is possible to replicate the correct dynamics of the system. To our knowledge this has up to now been restricted to very special cases (e.g., the period-doubling case) then it is preferable to use the L model. In cases where the deterministic dynamics is not known, or where there may be a stochastic model, then the P model may be preferable. An example of this is in fully developed turbulence where measurements corresponding to one- or two-dimensional cuts in three-dimensional space. There are also other reasons[10] which propel practitioners of tur-

bulence towards P models.

In Secs. V and VI we will analyze a variety of laboratory experiments via the transfer-matrix formalism. The reader is forewarned of the pitfalls of blind curve fitting. We will, however, show that by sensible choices of the model and the dynamical parameter a arising from physical arguments or Fourier spectra, one can get some of the information about the underlying multiplicative process from the experimentally determined D_q curves.

V. LABORATORY EXPERIMENTS IN RAYLEIGH-BÉNARD CONVECTION

Here we will reexamine the analysis of Feigenbaum *et al.* on the extraction of an underlying multiplicative process from the data of Glazier *et al.*[7] and that of Jensen *et al.*[9] and we illustrate the ambiguities in this extraction process. The data to be analyzed here are taken from the convection experiments in a small aspect-ratio cell.[8,7] An oscillatory instability sets in at a certain critical Rayleigh number in such flows. Subsequent increases in the Rayleigh number leads to chaotic fluid motion via the period-doubling scenario.[7] This is the first of the two situations we examine. If the oscillatory state is modulated by an independent external source, and if the modulation frequency is incommensurate with the flow oscillation frequency (in the presence of coupling), the fluid system undergoes transition to chaos via the quasiperiodic state. The data we analyze in this case corresponds to the frequency ratio set to the golden mean.[8]

A. Onset of chaos via the period doubling route

The period-doubling attractor is a paradigmatic example of chaotic dynamics and fractals. Since the dynamics of this route to chaos and the construction of this attractor are well understood, we consider this an excellent example to illustrate the points of this paper.

In an earlier paper, Feigenbaum *et al.*[6] demonstrated that one can extract from the Renyi dimensions, at least some of the basic length scales, the value of a, as well as information about the nature of the inflexion point (of the map). We would like to point out that, although the solutions they got were correct, they are not unique. In Fig. 13 we show a comparison of the D_q curve from the data of Glazier *et al.*[7] (which Feigenbaum *et al.* used to get their results) with the D_q curves of the period-doubling attractor generated from an L model represented by a 2×2 transfer matrix with $a=2$ and an L model represented by a 4×4 transfer matrix with $a=g$. We see that all of them agree quite well. If we did not know from other considerations that the underlying dynamics was of the period-doubling type we would not have any idea that $a=2$ and could just as well presume that $a=g$. The choice of $a=2$ is the correct one only because we know that it is so from other arguments, e.g., closest return times, etc.[21] We also show a comparison in Fig. 14, with a D_q curve generated by a P model represented by a 2×2 transfer matrix with $a=2$. The excellent agreement between the two curves indicates the equivalence between P models and L models.

We point out that we are comparing various fits with

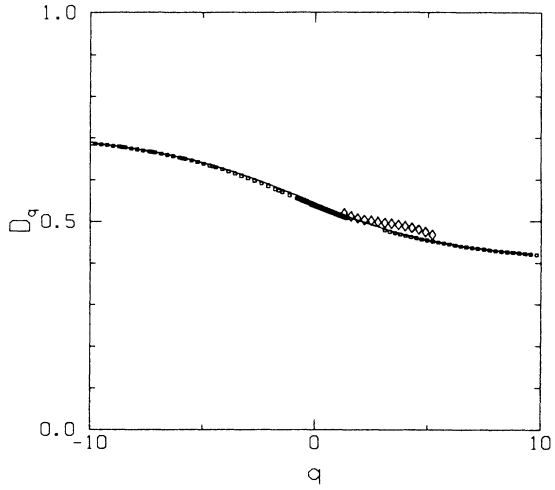

FIG. 13. The D_q curve for the period-doubling attractor (approximated by the curve generated by an L model with $a=2$, 4×4 TM (solid line) (where the four scales are the leading four scales of the Feigenbaum scaling function), compared with an L model with $a=g$, 4×4 TM (squares). The agreement is remarkable, showing that to a high precision it is not possible to discern the curves computed from different values of a. The diamonds show the experimental data from the Rayleigh Bénard experiments of Glazier *et al.* (Ref. 7). To get an idea of the error bars in the experimental data the reader is referred to Ref. 7. We are comparing the data with a three-scale approximation to the actual period-doubling D_q curve; the reason for this is discussed in Sec. V A of the text.

the D_q curve generated from an L model with $a=2$ represented by a 2×2 transfer matrix (i.e., a three-scale approximation) and not from the actual period-doubling attractor itself. There are two reasons for this. First, we know that $a=2$ from other considerations, and that the D_q curve generated from such a model is to within a few

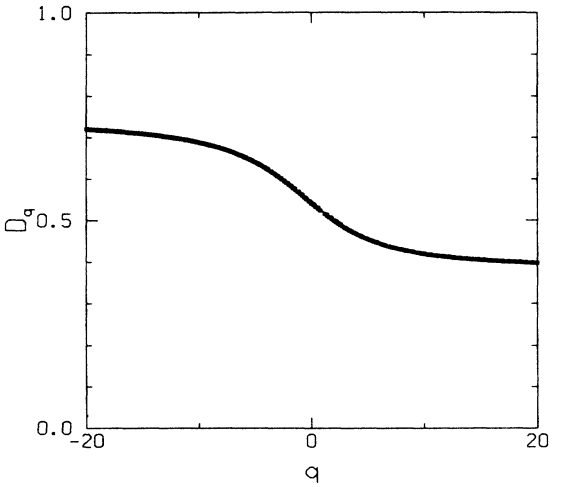

FIG. 14. The D_q curve for the period-doubling attractor compared with those from those generated L (squares) and P models (circles). The agreement shows that curves generated from L or P models are equivalent.

percent identical to the D_q curve of the period-doubling attractor;[22] second, our purpose here is not to show how successively refined models approximate the true D_q curve but that different models using the correct or the wrong values of a can give equally good fits. Similarly when we make circle-map comparisons in Sec. V B we will compare our fits not with the D_q curve of the actual circle-map attractor but with a three parameter model that has $a=g$. Once again the reasons are the same, the only difference being that for the circle map $a=g$.

B. Onset of chaos via the quasiperiodic route

Another important and well studied example, is the dynamics of the sine circle map when the dressed winding number is the golden mean. This is an example of the quasiperiodic route to chaos. We will later use the results of this section when we analyze the experiments of Olinger and Sreenivasan[11] done in the wake of an oscillating cylinder. In addition we will compare our results with those of Feigenbaum *et al.*[6] for similar quasiperiodic experiments in convection.

In Fig. 15 we show the $\tau(q)$ curve from the data of Jensen *et al.*, which was used by Feigenbaum *et al.*[6] for recovering information identical to the circle-map dynamics. Once again, we state that the solution listed by them in Ref. 6, though correct, is not unique. Motivation for the choice of $a=g$ must be found elsewhere. For the circle map, the Fourier spectra show clear peaks at powers of the golden mean, which can be taken as an indication of golden-mean dynamics, i.e., $a=g$. To show that one would otherwise not be able to decide the value of a, in Fig. 15 we also show fits to the D_q curve computed from an L model represented by a 2×2 transfer matrix with

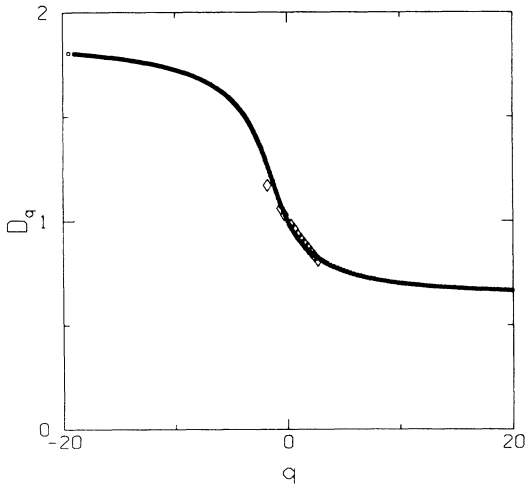

FIG. 15. Comparison of the D_q curve of the circle map at the golden-mean critical point [approximated by the curve generated by an L model (solid line) 4×4 TM, with $a=g$, which we know from closest return time arguments to be correct] with an L model with $a=2$, 2×2 TM. The agreement is remarkable, showing once again that to a high precision it is not possible to discern curves obtained from different values of a. The diamonds show the experimental data from the Rayleigh-Bénard experiments of Jensen *et al.* (Ref. 9).

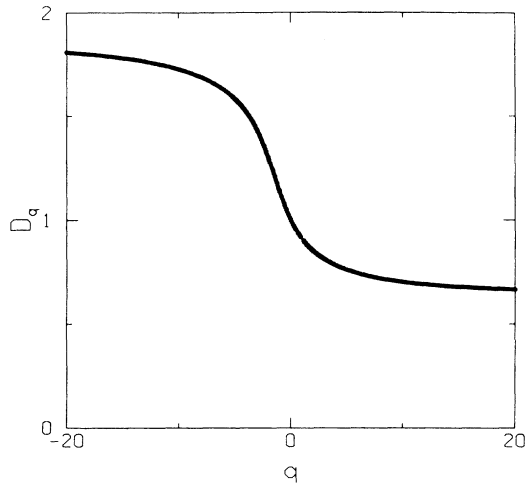

FIG. 16. The D_q curves from P (circles) and L models (squares) with $a=2$ using a 2×2 TM for the circle map at the golden-mean critical point. The agreement again shows that curves generated from L or P models are equivalent.

$a=2$, an L model represented by a 4×4 transfer matrix with $a=g$. Each of these models have exactly three free parameters. The fits in all three cases are excellent, and within the experimental error of the experimental data. In Fig. 16 we compare fits of D_q curves generated from an L model represented by a 2×2 transfer matrix with $a=2$ and a P model represented by a 2×2 transfer matrix with $a=2$. This comparison again shows that one cannot distinguish between P and L models through their D_q curves. Finally, in Fig. 17 we compare fits of D_q curves generated from an L model represented by a 2×2 transfer matrix with $a=2$ and an L model represented by

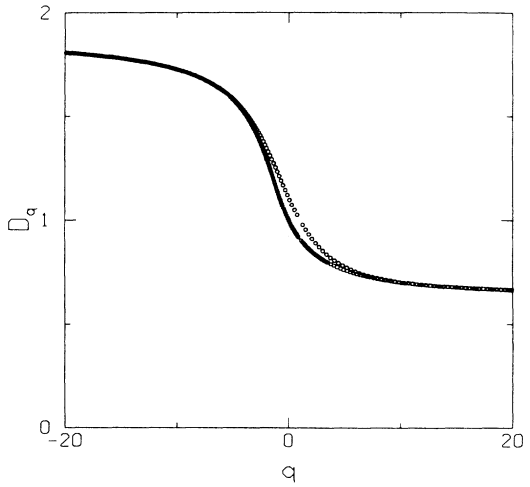

FIG. 17. The D_q curve from Fig. 15 [from an L model (solid line) 2×2 TM, with $a=2$], compared with that from an L model $a=g$, 2×2 TM (circles). This latter model has only two free parameters and thus one cannot fit the entire curve, indicating that at this level of refinement one would be led to believe that the dynamics was of the binary and not of the golden-mean kind.

a 2×2 transfer matrix with $a=g$. Clearly (at the 2×2 transfer-matrix stage), one is inclined to believe that the dynamics is of the binary variety and not of the golden-mean kind. This again tells us that simple curve fitting of the D_q and $f(\alpha)$ curves is not sufficient to tell us the value of a. The reason that an L model represented by a 2×2 transfer matrix with $a=g$ does not fit the D_q curve is that such a model has only two free parameters, while for $a=2$ the model has three. As already remarked, one only needs three free parameters to get good agreement with most D_q curves.

VI. LABORATORY EXPERIMENTS IN OPEN FLOWS

We will now apply this formalism to laboratory experiments in open-flow systems corresponding to two diverse circumstances. The first case consists of an attractor in phase space constructed from the velocity measured in the wake of an oscillating cylinder. The second case corresponds to the distribution in three-dimensional physical space of the turbulent energy dissipation in several flows (grid turbulence, wakes and boundary layers in both the laboratory and the atmosphere). In both cases we attempt to extract basic dynamical information of the underlying physical process.

A. Low Reynolds-number flow in the wake of an oscillating cylinder

Briefly, the flow analyzed is the wake of transversely oscillating circular cylinder of large aspect ratio (~300). The periodic vortex shedding behind the cylinder imparts, at a slightly supercritical Reynolds number, a periodic motion to the wake. The cylinder oscillation (usually quite small) provides another periodic component. The amplitude of the oscillation can be thought of as the motion-coupling parameter between the two oscillators. The flow can thus be thought of as a nonlinear system in which the natural vortex shedding is modulated by the oscillation frequency of the cylinder, generating in phase space a flow on a torus. The special case of interest is when the frequency ratio (oscillation frequency to the vortex shedding frequency) equivalent to the dressed winding number is the inverse of the golden mean, and the oscillation amplitude is set to the critical value corresponding to the breakdown of the two-torus. The flow Reynolds number is 55, the critical value being about 46.[23] By making detailed measurements at the Reynolds number of 55, Olinger and Sreenivasan[11] showed that the flow displays several features common to circle maps. For rational frequency ratios, Arnol'd tongues organized according to the Farey construction were found, with the behavior along the critical line approximating the devil's staircase structure. Associated with the quasiperiodic transition to chaos at the inverse golden-mean frequency ratio, spectral peaks at various Fibonacci sequences appeared (Fig. 18), and the measured D_q was found to be close to that of the sine circle map. The purpose here is to confirm this correspondence with the circle map via the thermodynamic formalism, and to extract the scaling

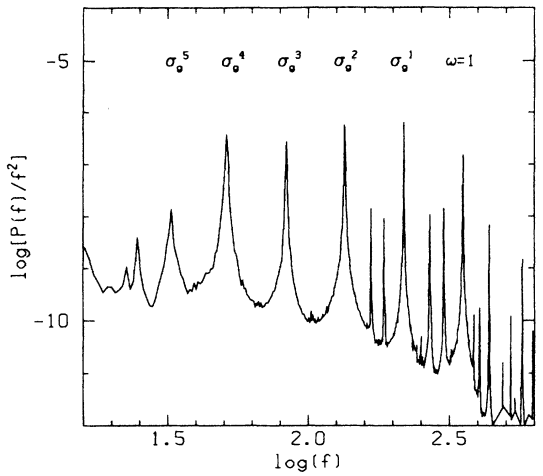

FIG. 18. The frequency-scaled power spectrum for velocity fluctuations in the wake of an oscillating cylinder near the critical golden-mean point (σ_g = golden mean).

information associated with the wake dynamics.

Although Olinger and Sreenivasan covered all accessible range of oscillation amplitudes and frequency ratios, our interest is specific to the case of golden-mean frequency ratio, and the critical oscillation amplitude at which chaos sets in due to the breakdown of the two-torus structure in phase space. The golden-mean ratio was achieved in the experiments to better than 0.1%. The Poincaré section was obtained by sampling data at minima of the measured velocity signal. The resulting Poincaré section was embedded in three dimensions using the usual time-delay methods[24] (in which it was nonintersecting in all three views), and a smoothened attractor was obtained by performing averages locally. Projections of the unsmoothened and smoothened attractor are shown in Figs. 19 and 20, respectively. The Renyi dimen-

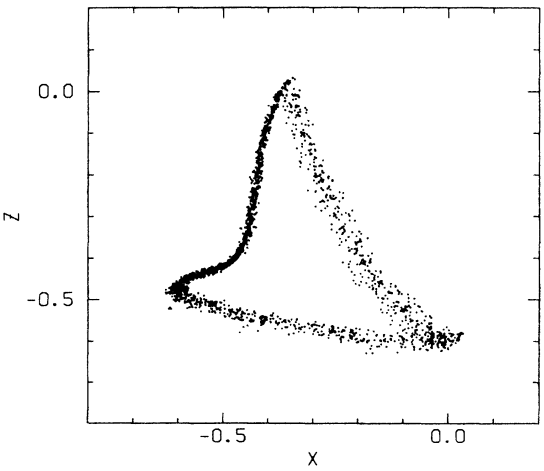

FIG. 19. A projection of the attractor for the velocity in the wake of the oscillating cylinder. The velocity signal (which corresponds to a Poincaré section of the attractor) is embedded in three-dimensional space to reconstruct the entire attractor using the usual time-delay method.

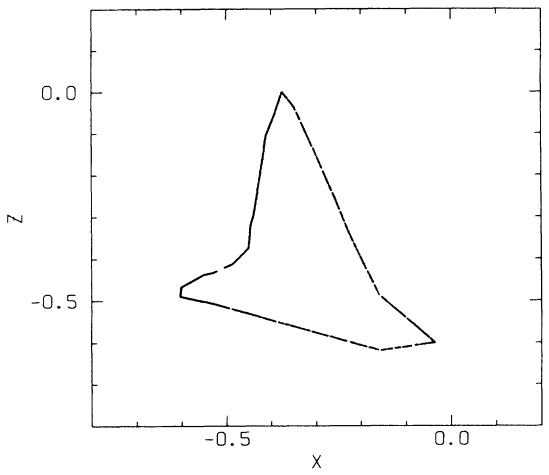

FIG. 20. The smoothened version of Fig. 19.

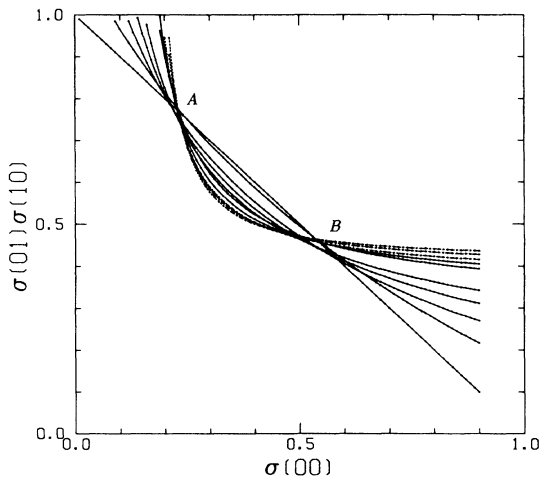

FIG. 21. Determining the scales $\sigma_l(00)$ and $\sigma_l(01)\sigma_l(10)$ from the D_q curve from the wake experiment.

sions D_q were obtained by using standard box-counting methods; in each case the scale similarity region in the appropriate log-log plots extended to about two decades. The multifractal spectrum $f(\alpha)$ was then calculated via Legendre transforms.

We make use only of a small subset of the data near $q=0$ (shown in Table I) where they are more reliable, and have ignored data for $q<0$ because of possible noise effects.[11] On the strength of the conclusions in Ref. 11 we attempt to solve the characteristic equation of (the lowest-order approximation to) the transfer matrix of the circle map. This means we will assume $a=g$. Motivation for this assumption comes from the Fourier spectra of the time signal that shows clear peaks at powers of the golden mean (Fig. 18), indicating golden-mean dynamics. We fix this value of a in the characteristic equation and in addition use the experimental fact that $D_0=1$ and plot a family of (intersecting) curves as a function of $\sigma_l(00)$ versus the product $\sigma_l(01)\sigma_l(10)$. Each of these curves corresponds to the solution at a different experimental τ of the characteristic equation. Recall the conclusion in Ref. 17 that in extracting information from thermodynamic quantities like the Renyi dimensions, one can do no better than extract $\sigma_l(01)\sigma_l(10)$ as a product. Different values of $\sigma_l(01)$ and $\sigma_l(10)$ that keep the product the same will yield identical D_q curves.

It is seen that the curves intersect in the vicinity of two regions marked A and B in Fig. 21. These intersections correspond to solutions of the characteristic equation of the transfer matrix. Both these solutions give two parameter fits to the D_q curve of the circle map. Note that the solutions corresponding to region B lead us to conclude that $\sigma_l(00)=0.47$ and the product $\sigma_l(01)\sigma_l(10)=0.53$. These are in excellent agreement with the theoretical values for the circle map which were found in Sec. V. Note, however, for reasons discussed earlier (with only two free parameters), only part of the D_q curve can be fitted at this level of approximation. We can in principle find higher-order scaling lengths and get better fits, but choose not to due so, in light of the accuracy of the experimental data.

TABLE I. A partial list of q versus τ values from the oscillating-cylinder experiment.

q	τ	q	τ
0.0	−1.000	1.8	0.7024
0.3	−0.686	2.1	0.944
0.6	−0.372	2.4	1.181
0.9	−0.091	2.7	1.423
1.2	0.178	3.0	1.658

B. Energy dissipation in fully turbulent flows

The physical quantity of interest here is the energy dissipation rate ε in fully turbulent flows, one of whose striking characteristics is its spatial intermittency. An example of a one-dimensional section through the energy dissipation field was shown in Fig. 2; the underlying dynamics is believed to be a cascading process of energy transfer from larger to smaller scales. It is therefore natural to expect that the distribution of the energy dissipation might possess self-similar scaling properties. This was indeed shown to be the case in Ref. 25 for one-dimensional sections of ε. In Ref. 10 it was further shown, by empirical comparisons of the experimental D_q and $f(\alpha)$ data with those of two-scale Cantor measures, that the dynamics leading to the observed multifractal distributions of ε can be well approximated by a single multistep process involving unequal energy distribution in the ratio $\frac{7}{3}$, the eddy size contraction at each step being equal. (As already mentioned, eddy subdivision into equal pieces is motivated by expectations that energy transfer tends to progress from one scale to the neighboring size. There is no conclusive justification for this assumption, but it is the simplest case to examine.) Our in-

tention here is to deduce this result via the formal transfer-matrix technique described in Sec. III, and to see if one can improve on the conclusions of Ref. 10.

The experimental data used in Ref. 10 were obtained (in the order of decreasing Reynolds number) in the atmospheric boundary layers several meters above the roof of a four story building, a laboratory turbulent boundary layer, the turbulent wake of a circular cylinder, and finally, a turbulent flow behind a square grid of round bars—the last three created in a wind tunnel. The Reynolds number (based on a characteristic oncoming mean velocity and an integral length scale) varied approximately between 10^4 and 10^7. More details can be found in Ref. 25, where it was shown that the measured D_q and $f(\alpha)$ data for ϵ were universal features of all fully turbulent flows. A partial list of the averaged D_q data is given in Table II.

Using the procedure described in Appendix A, we use the mean D_q data from these experiments to determine the primary scales p_1 and p_2 for a two-scale P model with no memory. From Fig. 22, which shows the result of such an effort, we conclude that p_1 and p_2 are close to 0.3 and 0.7. In particular the negative q's lead us to believe that p_1 is 0.3, while the positive q's agree better with the value of $p_1=0.29$. This small discrepancy may be due to the lesser reliability of high-q data.

A somewhat better fit to the data can be obtained by allowing both unequal L's and unequal P's (LP models), the formalism for which is described in Appendix B. We choose not to present the calculations here in view of the fact that such results are harder to interpret physically, and that the somewhat limited experimental accuracy does not at present justify such refinements.

The better fits to the D_q curve by the LP models can be understood purely in terms of the number of free parameters available. As already shown in the example of the two scale Cantor measure, the thermodynamics of LP models, where both L and P vary, can be replicated by L or P models with one time step memory (i.e., introducing one more free parameter). A D_q curve generated by an L model represented by a 2×2 transfer matrix with $a=2$ is shown in Fig. 23. The excellent agreement of the two curves is not unexpected in light of the discussion in Sec. IV. Here we would like to caution the reader that the only evident justification for assumption of a binary process by Meneveau and Sreenivasan[10] is that it is the simplest model that would to a good approximation replicate the observed statistical properties of the data. As shown here, it is only one of the *infinite* models that would give rise to the observed D_q curves. A D_q curve generated by an L model represented by a 4×4 transfer matrix with the $a=g$ (golden-mean dynamics) of the same data is shown in Fig. 24.

TABLE II. A partial list of q versus τ values of ϵ averaged from several fully turbulent flows.

q	τ	q	τ
−10.0	−17.70	0.0	−1.00
−8.0	−14.15	0.5	−0.45
−7.0	−12.27	2.0	0.79
−6.0	−10.50	3.0	1.40
−5.0	−8.72	4.0	1.92
−4.0	−7.02	5.0	2.46
−3.0	−5.34	6.0	2.92
−2.0	−3.75	7.0	3.38
−1.0	−2.29	10.0	4.81

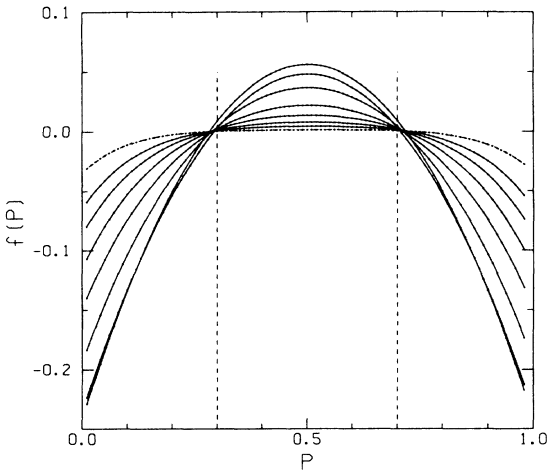

FIG. 22. Determining the scales $\sigma_p(0)$ and $\sigma_p(1)$ from the D_q curve for open flows (each curve corresponding to a different positive q from Table II). The D_q curve used corresponds to the mean of several such curves from different realizations as well as different flows. The dashed lines show the values of $\sigma_p(0)=0.3$ and $\sigma_p(1)=0.7$ which corresponds to a model proposed in Ref. 10.

VII. CONCLUSIONS

We have shown by a variety of examples, both theoretical and experimental, that the procedure of extracting dynamics from the thermodynamic data [the D_q or $f(\alpha)$

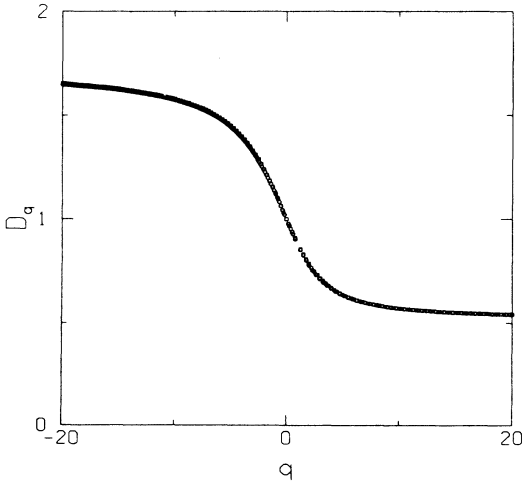

FIG. 23. A plot of D_q curves from an L model with $a=2$, 2×2 TM. The excellent fit shows that the earlier proposed P model (Ref. 10) is not the only possible fit to the data.

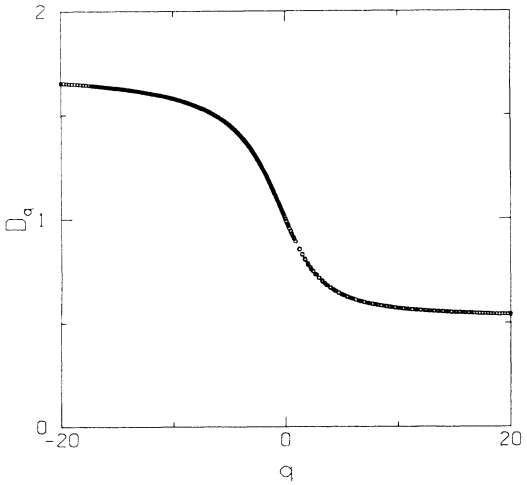

FIG. 24. A plot of D_q curves from an L model with $a=2$, 2×2 Tm and a P model with $a=g$, 4×4 TM. This shows that binary dynamics is not the only dynamics consistent with the data; golden-mean dynamics works just as well.

curves] is nonunique. However, if additional dynamical information can be brought to bear on the problem, one may in fact use the thermodynamic formalism to extract information about the underlying multiplicative process. We have examined several experimental circumstances from which dynamical models could be constructed. We warn the reader, however, that the additional information required to make a judicious choice among the infinity of possibilities is often nontrivial in nature.

ACKNOWLEDGMENTS

We are grateful to Charles Meneveau, Peter W. Jones, and Benoit B. Mandelbrot for many stimulating discussions throughout the various stages of this work. Useful discussions with Ganapathy Murthy and David Olinger are also acknowledged. This work was supported by grants from the National Science Foundation and U.S. Air Force Office of Scientific Research.

APPENDIX A

In this appendix we will outline some details of how the thermodynamic quantities D_q are calculated for the various models discussed in this paper. For the first half of this Appendix will draw heavily from the work of Feigenbaum.[17]

1. L models

We first consider a binary process where each piece splits into two pieces at the next level of refinement. Denote the left piece by the number 0 and the right piece by the number 1. Further, consider a process that has a one time step or one level memory, i.e., it remembers if its parent was a left or right offspring. Thus for the purpose of deciding the contraction ratio it will undergo, each piece can be encoded by two binary digits. The first digit denotes whether the interval itself was a left or right offspring, and the second digit denotes whether its parent was itself a left or right offspring. Thus we have a total of four different contracting scales. Denote these length contraction ratios by $\sigma_l(00)$, $\sigma_l(01)$, $\sigma_l(10)$, and $\sigma_l(11)$, respectively. Then following the procedure described in Refs. 17 and 6 and in Sec. III of the text we can denote such a process by a 2×2 transfer matrix,

$$T=\begin{bmatrix}\sigma_l^{-\tau}(00) & \sigma_l^{-\tau}(01)\\ \sigma_l^{-\tau}(10) & \sigma_l^{-\tau}(11)\end{bmatrix}. \tag{A1}$$

The characteristic equation of this transfer matrix is simply Eq. (24). Now writing λ as a^q, we get

$$a^{2q}-[\sigma_l^{-\tau}(00)+\sigma_l^{-\tau}(00)]a^q + [\sigma_l^{-\tau}(00)\sigma_l^{-\tau}(11)-\sigma_l^{-\tau}(01)\sigma_l^{-\tau}(10)]=0 . \tag{A2}$$

Remembering that

$$\tau(q)=(q-1)D_q , \tag{A3}$$

we now have an equation that relates the fundamental length contraction ratios with D_q and q. It is important to note that we are constraining ourselves to a binary process with only one time step or one level memory. Restricting ourselves to such a model is not as bad as it may seem at first sight because it seems that chaotic systems, at least the ones at the onset of chaos, have memories that die off exponentially.[6] Thus considering an n time step or n level memory would have an exponentially small correction with increasing n. For such a 2×2 matrix, the requirement that $\tau=0$ for $q=1$, restricts the possible values a to 0, 1, $(\sqrt{5}+1)/2$ and 2, of which 0 and 1 are trivial values. The value of a is the golden mean when $\sigma_l(11)=0$ [see Eq. (A2)]. One of the points this paper makes is that at least to experimental accuracy, it really does not matter which of the nontrivial values of a one uses.

We can use Eq. (A2) for two purposes. First consider a situation where we know the four length ratios and would like to calculate the D_q curve. Then if all the four length scales were nonzero we would use $a=2$, substitute the length contraction ratios in the equation, and simply solve the equation for $\tau(q)$ by choosing different values of q. This then gives the desired $\tau(q)$ curve. Notice that the $\tau(q)$ curve depends only on four parameters a, $\sigma_l(00)$, $\sigma_l(11)$, and the product $\sigma_l(01)\sigma_l(10)$. Changing the values of $\sigma_l(01)$ and $\sigma_l(10)$ in such a way as to keep their product constant would yield the same $\tau(q)$ curve. This degeneracy has been emphasized before by Feigenbaum and reminds us the D_q is a macroscopic average and not a microscopic quantity. Furthermore, one should remember that at this level of approximation (one level memory) we have no choice for a. It will be 2 unless $\sigma_l(11)$ is zero, in which case it will be equal to the inverse of the golden mean g.

As an aside let us note that one can actually make the computations somewhat simpler[17] for the model we have considered if we instead choose a value of τ and compute

the value of q associated with it. Note that the characteristic equation for the eigenvalue of a 2×2 transfer matrix is a quadratic equation. Then the leading eigenvalue of T is given by

$$\lambda(-\tau)=\frac{\sigma_l^{-\tau}(00)+\sigma_l^{-\tau}(11)}{2}+\left[\left[\frac{\sigma_l^{-\tau}(00)-\sigma_l^{-\tau}(11)}{2}\right]^2+\sigma_l^{-\tau}(01)\sigma_l^{-\tau}(10)\right]^{1/2}. \quad \text{(A4)}$$

Remembering that $\lambda=a^q$, we have

$$q=\log(\lambda)/\log(a) . \quad \text{(A5)}$$

Then we can compute D_q from Eq. (A3).

Now consider the reverse situation. Given an arbitrary τ versus q curve can we find the matrix elements that would generate it? First, let us note that there is no reason that one should be able to find a solution of the form dictated by considering a binary process with a single step memory. However, it turns out that for all the cases considered in this paper we can. In addition we find solutions both for $a=2$ and $a=g$. To do this we consider the D_q curves at three points D_∞, $D_{-\infty}$, and D_0. Then using the relations

$$D_\infty=\log[\sigma_p(00)]/\log[\sigma_l(00)] , \quad \text{(A6)}$$

$$D_{-\infty}=\log[\sigma_p(11)]/\log[\sigma_l(11)] , \quad \text{(A7)}$$

and by substituting $q=0$ (which implies $\tau=-D_0$) in Eq. (A2) gives

$$1-[\sigma_l^{D_0}(00)+\sigma_l^{D_0}(11)]+\sigma_l^{D_0}(00)\sigma_l^{D_0}(11)-\sigma_l^{D_0}(01)\sigma_l^{D_0}(10)=0 . \quad \text{(A8)}$$

Thus using Eqs. (A6)–(A8) we can calculate the three parameters, $\sigma_l(00)$, $\sigma_l(11)$, and $\sigma_l(01)\sigma_l(10)$, required to generate a $\tau(q)$ curve from a binary one time-step model.

If, however, $\sigma_l(11)=0$, then from Eq. (A2) one requires $a=g$. The transfer matrix is

$$T=\begin{bmatrix}\sigma_l^{-\tau}(00) & \sigma_l^{-\tau}(01\\ \sigma_l^{-\tau}(10) & 0\end{bmatrix} , \quad \text{(A9)}$$

i.e., we have only two free parameters $\sigma_l(00)$ and the product $\sigma_l(01)\sigma_l(10)$. We can thus find these values by using any two of the three relations, Eqs. (A6)–(A8). We find, however, that the fit will not be good for most of the curves considered in this paper. This is because one needs at least three free parameters to get good fits to these D_q curves. To construct a model with one more free parameter, one must go to the next order of the transfer matrix. This means we now consider a two level memory, each piece remembering if its parent and its grandparent were left or right pieces. Each piece thus decides its contraction ratio through a three digit binary sequence. Remembering that the 11 transition is forbidden, the transfer matrix then reads as[6]

$$T=\begin{bmatrix}\sigma_l^{-\tau}(000) & \sigma_l^{-\tau}(001) & 0 & 0\\ 0 & 0 & \sigma_l^{-\tau}(010) & 0\\ \sigma_l^{-\tau}(100) & \sigma_l^{-\tau}(101) & 0 & 0\\ 0 & 0 & 0 & 0\end{bmatrix} . \quad \text{(A10)}$$

Here each element is specified by its time history at three time steps, t_{n+1}, t_n, and t_{n-1}. Thus $\sigma_l(010)$ would be the contraction ratio of an interval designated by (01) contracting onto an interval designated by (10). Since the first digit of the first pair $(t_n,t_{(n-1)})$ will always equal the last digit of the second pair $(t_{(n+1)},t_n)$, one simply contracts the two pairs and writes it as a single three digit number. The forbidding of two successive 1's makes the matrix sparse so that there are only three free parameters that determine the $\tau(q)$ curve. We get these from the values of D_∞, $D_{-\infty}$, and D_0, where now $a=g$. Having arrived at a three-parameter equation for the golden-mean dynamics we find that we can once again get good fits to all the $\tau(q)$ curves constructed in this paper.

B. *P* models

The equations for computing $\tau(q)$ curves from P models is similar to those for L models with a few twists. Consider once again a one time-step memory binary model, the transfer matrix for which is

$$T=\begin{bmatrix}\sigma_p^q(00) & \sigma_p^q(01)\\ \sigma_p^q(10) & \sigma_p^q(11)\end{bmatrix} . \quad \text{(A11)}$$

But now we have two additional conservation equations,

$$\sigma_p(00)+\sigma_p(10)=1 \quad \text{(A12)}$$

and

$$\sigma_p(01)+\sigma_p(11)=1 . \quad \text{(A13)}$$

These equations simply represent the conservation of probability of each sub branch in the tree. They imply that only two of the four elements of T are independent. Therefore for a three-parameter fit to the D_q curve we need to use one more piece of information. This is obtained from the Hausdorff dimension of the support of the measure. For although each of the pieces are of equal length, their length will be dependent of the value of D_0. In particular, at the nth stage the intervals must satisfy the equation

$$\sum_{i=1}^{N_n}(L_i^{(n)})^{D_0}=1 . \quad \text{(A14)}$$

Now assume, (consistent with our model) that at each level of refinement, each interval splits into two smaller pieces each shrinking by some constant ratio b. Then at the nth level there will be a total of 2^n intervals each of length b^{-n}. Thus Eq. (A14) becomes

$$\sum_{i=1}^{2^n}(b^{-nD_0})=2^n b^{-nD_0}=1 . \quad \text{(A15)}$$

Knowing D_0 we can solve for b. Once again in analogy to the L model, we need three free parameters [$\sigma_p(00)$, $\sigma_p(11)$, and b] which are present in the 2×2 transfer-matrix representation of the P model (where none of its elements are zero). Given these three parameters we can generate a $\tau(q)$ curve using the characteristic equation of the transfer matrix which is

$$\lambda(q)=\frac{\sigma_p^q(00)+\sigma_p^q(11)}{2}+\left[\left[\frac{\sigma_p^q(00)-\sigma_p^q(11)}{2}\right]^2+\sigma_p^q(01)\sigma_p^q(10)\right]^{1/2}. \quad \text{(A16)}$$

Since $\lambda=b^{-\tau}$, we have

$$\tau=-\log(\lambda)/\log(b)\ , \quad \text{(A17)}$$

which enables us to compute $\tau(q)$ from our knowledge of [$\sigma_p(00)$, $\sigma_p(11)$, and b].

Conversely, given a D_q curve one could use any three points on it to determine the three parameters that represent the binary model. The simplest way would be, given D_∞, $D_{-\infty}$, and D_0 one could use the relations

$$D_\infty=\log[\sigma_p(00)]/\log(b^{-1})\ , \quad \text{(A18)}$$

$$D_{-\infty}=\log[\sigma_p(11)]/\log(b^{-1})\ , \quad \text{(A19)}$$

and Eq. (A15) to find $\sigma_p(00)$, $\sigma_p(11)$, and b.

To replicate the golden-mean dynamics, one lets $\sigma_p(11)=0$ (which then makes $b=g$ when $D_0=1$). Computing the desired $q(\tau)$ curve for this model is done in the same way for the models possessing binary dynamics. Just as in the L-model case this restriction reduces the number of free parameters to two. One then needs to go to a 4×4 transfer matrix, i.e., a model with two time steps memory to have three free parameters. The calculation of the D_q curve can then be done the same way as in the binary dynamics case.

An important point that the reader should note is that these models can be refined to greater complexity and the fits to the D_q curves made arbitrarily accurate simply by increasing the number of free parameters. However, in all of the fits shown in this paper, we have chosen to use models with at most three free parameters, and used the values of D_∞, $D_{-\infty}$, and D_0 to find them. The D_q curves generated from an underlying multiplicative process defined from these three parameters were then used to fit the data from experiments. The reason for such good agreement over the entire curve is unexpected and not well understood. The remarkable agreement however obviates the need to consider more refined models.

APPENDIX B: GENERALIZED CANTOR MEASURES (*LP* PROCESSES)

It is easy to adapt this formalism to the case of fractal measures living on fractal sets. In the simplest two-scale case, one can consider a unit interval splitting into two pieces of unequal length. However, rather than giving the two pieces the same probability, we assign them unequal probabilities p_1 and p_2. This process is then repeated, and is similar to the well known *(contracting) Bakers transformation*. We now elaborate on the thermodynamics of the partition function where both L_i and P_i vary. We can define two variables, $E_i=-\ln(L_i)$ and $\beta V_i=-\ln(P_i)$. Then the partition function can be written as[26,27]

$$\Gamma(q,\tau)=\sum_i (P_i)^q/(L_i)^\tau=\sum \exp[-\beta(E_i-pV_i)]\ , \quad \text{(B1)}$$

i.e., we are making the following identifications of $\tau=\beta$ and $q=-p$. Then

$$\Gamma(q,\tau)=\exp[-G(\beta,p)]\ , \quad \text{(B2)}$$

where we have absorbed the β in the definition of G. There is nothing special about our choice of variables, one can use any conjugate pair of thermodynamic variables. The fractal dimension of the set, then corresponds to the value of $-\beta$ that makes $G(\beta,p)$ zero.[26]

One can also derive the appropriate transfer matrix with a view of extracting the relevant multiplicative process. In such a case it is convenient to use both the scaling functions (σ_l and σ_p) defined in the previous sections. Similar manipulations as used for the L and P models lead to a transfer matrix of the form

$$T=\begin{bmatrix}\sigma_p^{+q}(00)/\sigma_l^{-\tau}(00) & \sigma_p^{+q}(01)/\sigma_l^{-\tau}(01)\\ \sigma_p^{+q}(10)/\sigma_l^{-\tau}(10) & \sigma_p^{+q}(11)/\sigma_l^{-\tau}(11)\end{bmatrix}, \quad \text{(B3)}$$

where the leading eigenvalue is 1. The relevant quantities are once again found by solving the characteristic equation of this matrix. This is more complicated as we now deal with more variables, and multidimensional root-finding methods tend to become rapidly unstable as we go to higher-order approximations.

The problem with this model is that one does not know how to choose the partitions correctly except in some special cases. Thus in principle one almost always works with either the L or P model.

[1]B. B. Mandelbrot, *The Fractal Geometry of Nature* (Freeman, New York, 1977).

[2]U. Frisch and G. Parisi, in *Turbulence and Predictability of Geophysical Flows and Climate Dynamics*, Course LXXXVII of *Proceedings of the International School of Physics Enrico Fermi*, edited by M. Ghil, R. Benzi, and G. Parisi (North-Holland, New York, 1985).

[3]T. C. Halsey, M. H. Jensen, L. P. Kadanoff, I. Procaccia, and B. I. Shraiman, Phys. Rev. A **33**, 1141 (1986).

[4]A. Renyi, *Probability Theory* (North-Holland, Amsterdam, 1970).

[5]H. G. E. Hentschel and I. Procaccia, Physica **8D**, 435 (1983).

[6]M. J. Feigenbaum, M. H. Jensen, and L. Procaccia, Phys. Rev. Lett. **57**, 1507 (1986).
[7]J. A. Glazier, M. H. Jensen, A. Libchaber, and J. Stavans, Phys. Rev. A **34**, 1621 (1986).
[8]J. Stavans, F. Heslot, and A. Libchaber, Phys. Rev. Lett. **55**, 596 (1985).
[9]M. H. Jensen, L. P. Kadanoff, A. Libchaber, I. Procaccia, and J. Stavans, Phys. Rev. Lett. **55**, 25 (1985).
[10]C. Meneveau and K. R. Sreenivasan, Phys. Rev. Lett. **59**, 797 (1987).
[11]D. Olinger and K. R. Sreenivasan, Phys. Rev. Lett. **60**, 797 (1988).
[12]P. Billingsley, *Ergodic Theory & Information* (Wiley, New York, 1965).
[13]G. Bouligand, Bull. Sci. Math. II **52**, 320 (1928); **52**, 361 (1928).
[14]S. K. Sarkar, Phys. Rev. A **36**, 4104 (1987).
[15]D. Ruelle, *Thermodynamic Formalism, Encyclopedia of Mathematics and Its Applications* (Addison-Wesley, Reading, MA, 1978), Vol. 5.
[16]E. Aurell, J. Stat. Phys. **47**, 439 (1987).
[17]M. J. Feigenbaum, J. Stat. Phys. **46**, 919 (1987).
[18]B. B. Mandelbrot, J. Fluid. Mech. **62**, 331 (1974).
[19]E. B. Vul, Y. G. Sinai, and K. M. Khanin, Russ. Math. Surv. **39**, 1 (1984).
[20]M. J. Feigenbaum, J. Stat. Phys. **25**, 669 (1978).
[21]M. J. Feigenbaum, *Statistical and Particle Physics*, in Proceedings of the 26th Scottish Summer School in Physics, Scotland, 1984, edited by K. C. Bowler and A. J. McKane (Scottish Universities, Scotland, 1984).
[22]M. J. Feigenbaum, J. Stat. Phys. **46**, 925 (1987).
[23]K. R. Sreenivasan, P. J. Strykowski, and D. J. Olinger, in *Forum on Unsteady Flow Separation, FED* (American Society of Mechanical Engineers, New York, 1986), Vol. 52, pp. 1–14.
[24]J. P. Eckman and D. Ruelle, Rev. Mod. Phys. **57**, 617 (1985).
[25]C. Meneveau and K. R. Sreenivasan, Nucl. Phys. B (Proc. Suppl.) **2**, 49 (1987).
[26]T. Tél, Z. Naturforsch **43a**, 1154 (1988).
[27]M. Kohomoto, Phys. Rev. A **38**, 1345 (1988).